Received: 20 April 2023 | Revised: 22 September 2023 | Accepted: 5 October 2023

DOI: 10.1111/aor.14665

Artificial Organs WILEY

MAIN TEXT

Computational fluid dynamics-based design and in vitro characterization of a novel pediatric pump-lung

Dong Han[1] | Jiafeng Zhang[1] | Ge He[1] | Bartley P. Griffith[1] | Zhongjun J. Wu[1,2]

[1]Department of Surgery, University of Maryland School of Medicine, Baltimore, Maryland, USA

[2]Fischell Department of Bioengineering, A. James Clark School of Engineering, University of Maryland, College Park, Maryland, USA

Correspondence
Zhongjun J. Wu, Department of Surgery, University of Maryland School of Medicine, 10 South Pine Street, MSTF 436, Baltimore, MD 21201, USA.
Email: zwu@som.umaryland.edu

Funding information
National Institutes of Health, Grant/Award Number: R01HL118372, R01HL141817 and R01HL162940

Abstract

Background: Although extracorporeal membrane oxygenation (ECMO) has been used to provide temporary support for pediatric patients suffering severe respiratory or cardiac failure since 1970, ECMO systems specifically designed for pediatric patients, particularly for long-term use, remain an unmet clinical need. We sought to develop a new pediatric ECMO system, that is, pediatric pump-lung (PPL), consisting of a unique cylinder oxygenator with an outside-in radial flow path and a centrifugal pump.

Methods: Computational fluid dynamics was used to analyze the blood fluid field for optimized biocompatible and gas exchange performances in terms of flow characteristics, hemolysis, and gas transfer efficiency. Ovine blood was used for in vitro hemolysis and gas transfer testing.

Results: Both the computational and experimental data showed that the pressure drop through the PPL's oxygenator is significantly low, even at a flow rate of more than 3.5 L/min. The PPL showed better hemolysis performance than a commercial ECMO circuit consisting of the Quadrox-iD pediatric oxygenator and the Rotaflow pump at a 3.5 L/min flow rate and 250 mm Hg afterload pressure. The oxygen transfer rate of the PPL can reach over 200 mL/min at a flow rate of 3.5 L/min.

Conclusions: The PPL has the potential to provide adequate blood pumping and excellent respiratory support with minimal risk of hemolysis for a wide range of pediatric patients.

KEYWORDS

CFD, ECMO, gas transfer, hemolysis, in vitro, pediatric pump-lung

1 | INTRODUCTION

Respiratory failure is the most common cause of morbidity and mortality in the pediatric population. In 2016, respiratory distress ranked top 10 causes of infant death, according to data from the National Center for Health Statistics.[1] Respiratory failure is the leading reason for admission of children into pediatric intensive care units (PICU). In addition, it is also common in post cardiac surgery settings to have pre-operative elevated pulmonary vascular resistance, prolonged operative times, and ventricular failure. As respiratory status worsens, patients may develop acute respiratory distress syndrome (ARDS), with a reported rate

of 10.4% for PICU admissions.[2] Mortality for pediatric ARDS patients varies from 18% to 60%,[2,3] with underlying diseases including pneumonia, sepsis, aspiration, and trauma. Acute respiratory failure in children is frequently associated with pulmonary infections. According to the World Health Organization (WHO), more than 0.7 million children under 5 years of age died from acute respiratory failure caused by pneumonia in 2019, accounting for 14% of all deaths in children in that age range.[4]

Mechanical ventilation and extracorporeal membrane oxygenation (ECMO) are commonly used to treat pediatric patients with respiratory failure.[5,6] In spite of advances in mechanical ventilation techniques and selective antibiotic use, prolonged ventilator support is associated with poor outcomes such as infection, lung injury, delayed weaning, and increased mortality.[2,3] ECMO is a life-saving treatment technique that generally consists of a blood pump and an oxygenator, allowing the pumping and oxygenation of blood outside the body. Over the past several decades, the use of ECMO in pediatric patients has become a well-established therapy in the management of pediatric respiratory and cardiac failure.[7] According to the ELSO Registry, more than 70 000 pediatric and neonatal patients received ECMO support worldwide for pulmonary/cardiac failure up to 2022.[8] ECMO is easy to establish emergently without a major surgical procedure and is often preferred early after heart surgery when the heart and/or lungs are stressed and cannot adequately support the child.

Excellent short- and medium-term outcomes of ECMO support have been demonstrated in the literature.[9] However, current ECMO systems may be unsuitable for long-term use because gas exchange takes precedence over biocompatibility, and they all require aggressive anticoagulation therapy. With newer devices and improved components, including consoles, pumps, oxygenators, and cannulas, long-term ECMO support has been explored to sustain the sickest patients while they wait for a suitable lung transplant. However, compared with adult patients, pediatric patients pose unique challenges for ECMO use due to their complex anatomy and physiology. It has been suggested that the high mechanical shear stress generated by pumping flow through the ECMO circuit can damage blood components, leading to severe complications, such as hemolysis, thrombosis, and hemorrhage, in patients.[10,11] Although the pressure drop in the ECMO circuit varies by manufacturer, it is often considered too high for pediatric use. A high pressure drop requires a strong pumping action of the blood, resulting in high mechanical shear stress and increasing the risk of thrombus and clot formation.[12] Cases of ECMO replacement are much higher in children than in adults.[13] Therefore, a comprehensive understanding of blood fluid dynamics in the ECMO circuit is critical to optimizing pediatric ECMO therapy and minimizing adverse events.

Computational fluid dynamics (CFD) analysis has been widely used to assess and optimize blood flow in blood-contacting biomedical devices over the last two decades. It provides detailed insight into hemodynamic performance, unfavorable flow characteristics, and regions with high shear stresses. In conjunction with the CFD analysis, the power-law model, which correlates hemolysis with shear stress and exposure time, has been used to empirically assess red blood cell damage.[14,15] In recent years, the use of CFD to evaluate platelet activation is also one of the emerging topics to investigate platelet damage potential and biocompatible performance related to coagulation in blood-contacting medical devices.[16] CFD analysis has also been used for evaluating gas transfer performance during the design stage of blood oxygenators. Such numerical approaches can be economically advantageous prior to the fabrication of true prototypes.[17]

In this article, we present the development of a novel pediatric pump-lung (PPL) for ECMO through a combination of CFD design optimization and in vitro experimentation. The PPL was designed based on the CFD analysis of hydrodynamics and hemolysis in the pump and the gas transfer performance of the oxygenator. Ovine blood was used for the in vitro experiments. The hemolytic performance of the PPL was compared with an ECMO circuit consisting of the Quadrox-iD pediatric oxygenator and the Rotaflow pump (Getinge, Gothenburg, Sweden) under a clinically relevant condition, for example, venoarterial-ECMO, of 3.5 L/min flow rate and 250 mm Hg afterload pressure.

2 | PEDIATRIC PUMP-LUNG

The PPL is intended for pediatric patients (4 to 11 years old) with body weights ranging from 15 to 35 kg. It can be operated to generate a flow rate from 1.0 to 4.0 L/min with an efficient gas transfer rate and adequate afterload pressure. The conceptual PPL consists of a centrifugal blood pump and a cylindrical oxygenator, as shown in Figure 1. They are integrated by a connector (Figure 2). The blood inlet and outlet can be connected to 3/8-inch tubing. A shrouded impeller is utilized for the pump and supported by a single cup-and-ball hybrid magnetic/hydrodynamic bearing. Permanent magnets are enclosed inside the impeller and coupled with the outside driving magnets, which are mounted on the shaft of an external motor. The magnetic coupling force between magnets in the impeller

and motor maintains the balance and stability of the impeller. The pump has two blood flow paths, including a primary flow path from the axial inlet to the tangential outlet and secondary flow paths that surround the impeller in the gaps between the rotating impeller and housing.

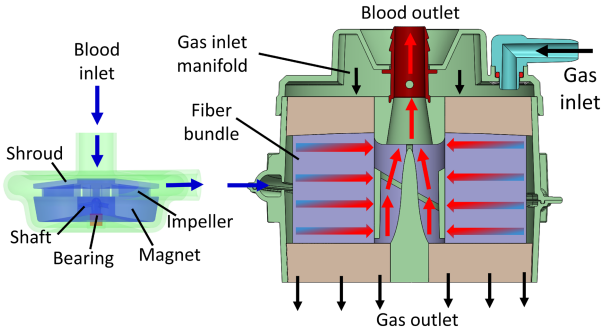

FIGURE 1 Schematic diagram of the cross-section of the designed pediatric pump-lung (PPL). [Color figure can be viewed at wileyonlinelibrary.com]

The primary flow path is responsible for generating the primary pressure head and pumping the blood to the oxygenator. The secondary flow path separates the rotating impeller from the stationary pump housing.

The oxygenator has a circumferential-radial outside-in blood flow path design achieved by a progressive spiral volute that wraps 270 degrees around the housing. This special design allows a uniform blood discharge across the outer surface of the fiber bundle. Blood can then flow uniformly and radially through the fiber bundle. A flow deflector in the center of the fiber bundle is configured to direct blood flow to the outlet of the oxygenator and prevent blood stagnation and recirculation. The fiber bundle is made from polymethylpentene (PMP) hollow fiber membranes (HFM) (Oxyplus, 3 M Membrana, Wuppertal, Germany) with an inner diameter of 23 mm, an outer diameter of 75 mm, and a length of 36 mm. The surface area of the fiber bundle is 0.83 m^2. The configuration and component arrangement for the PPL were adapted from

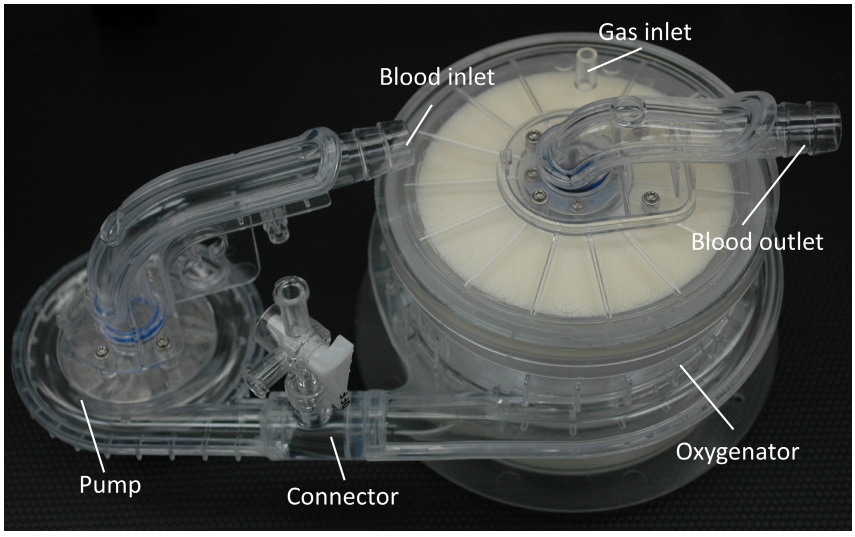

FIGURE 2 Image of an actual PPL. [Color figure can be viewed at wileyonlinelibrary.com]

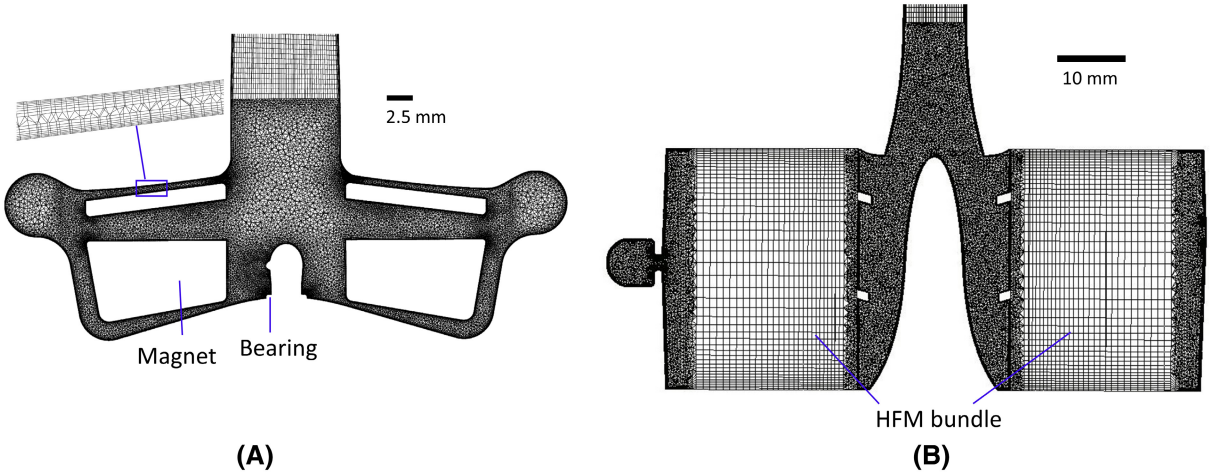

FIGURE 3 Meshing schemes in the (A) pump and (B) the oxygenator.

our previous adult oxygenator design.[18] CFD simulation-based analysis and design were performed with an iterative process to achieve the specified pump performance and gas exchange target while eliminating regions of high shear stress and adverse blood stasis. Finally, the computationally designed PPL was divided into individually manufacturable components. The prototypical PPL was fabricated and tested for its performance through in vitro experiments.

3 | COMPUTATIONAL FLUID DYNAMICS ANALYSIS AND DESIGN

The three-dimensional (3D) geometric model of the PPL was created using the 3D computer aid design (CAD) software package (Solidworks, v2018, Waltham, MA, USA). Fluid domains were extracted from the CAD files using Ansys Design modeler 19.2 (Ansys Inc., Canonsburg, PA, USA), and meshes were created using Ansys Meshing. The mesh elements in the regions with complex flow patterns and/or potentially high shear stresses were refined, and the flow region adjacent to the walls was meshed with inflation layers to allow more accurate prediction of the boundary layers. Figure 3 shows the cross-sectional view of the meshing scheme in the pump and oxygenator. A mesh sensitivity analysis was performed prior to simulation to ensure that the simulation results were independent of further mesh refinement.[19] A total number of 8.5 million cells was generated for the pump and a total number of 10 million cells for the oxygenator.

Numerical simulations were performed using the unstructured finite-volume-based CFD solver FLUENT 19.2 (ANSYS Inc., Canonsburg, PA). The rotation of the pump impeller was modeled using the multiple reference frame (MRF) approach. Blood was considered an incompressible Newtonian fluid with a density of 1050 kg/m^3 and a viscosity of 0.0035 kg/ms. The semi-implicit method for pressure-linked equations (SIMPLE), a pressure–velocity coupling scheme with second-order accuracy, was used to solve all fluid-governing equations with Menter's shear stress transport (SST) k-ω model. The volumetric flow rate was prescribed as the inlet boundary condition, and zero pressure was set as the outlet boundary condition. Navier-Stokes equations govern the blood flow,

$$\rho\left[\partial \boldsymbol{u} / \partial t + (\boldsymbol{u} \cdot \nabla)\boldsymbol{u}\right] = \mu \nabla^2 \mathrm{u} - \nabla p + \rho \boldsymbol{g} \tag{1}$$

where $\boldsymbol{u}$ is the velocity field of the fluid, t is time, μ is dynamic viscosity, ρ is density, p is pressure, and $\boldsymbol{g}$ is external body force.

3.1 | Hemolysis model

High shear stress is thought to damage erythrocytes and lead to hemolysis. The hemolysis index (HI), which quantifies the potential for hemolysis and is an index of device biocompatibility, was determined based on the conventional power-law hemolysis model,

$$HI(\%) = C\tau^{\alpha} t^{\beta} \tag{2}$$

where $C = 1.228 \times 10^{-5}$, $\alpha = 1.9918$ and $\beta = 0.6606$ for ovine blood.[20] τ is the scalar shear stress (SSS) defined as a von Mises-like stress,[14]

$$\tau = \left[\frac{1}{12}\sum\left(\tau_{ii} - \tau_{jj}\right)^2 + \frac{1}{2}\sum \tau_{ij}^2\right]^{1/2} \tag{3}$$

where τ_{ij} is the shear stress tensor with the $i \neq j$ rule applied in the above equation. By implementing the power-law model in the CFD simulation using the Eulerian scalar transport approach, HI (%) was calculated at the outlet, as described in detail in Refs. [15,21].

3.2 | Gas transfer model

Gas transfer analysis was performed on the oxygenator with the HFM bundle, whereas the flow domain was modeled as a single porous material approximated by the Ergun equation with a porosity of 0.5. Blood transport in the HFM bundle was modeled as a convection-diffusion-reaction process. The gas transfer evaluation was achieved by incorporating the gas diffusion and convection processes in the HFM into the CFD simulation,[17]

$$\boldsymbol{u}\left[\alpha \nabla P_{O_2} + [C]_H \nabla S\left(P_{O_2}\right)\right] = \alpha \cdot D \cdot \nabla^2 P_{O_2} + k_c A\left(P_{O_2}^G - P_{O_2}\right) \tag{4}$$

where P_{O_2} is the partial pressure of oxygen in blood and $P_{O_2}^G$ is the partial pressure of oxygen measured under atmospheric pressure. D is the oxygen diffusion coefficient in the fiber. α is the oxygen solubility in blood. k_c is the fiber mass transport coefficient. $[C]_H$ is the hemoglobin concentration. S is oxyhemoglobin saturation (SO_2), which is a function of PO_2.

The mass transfer rate $\dot{m}_{O_2}$, that is, O_2 transfer rate is calculated according to the averaged PO_2 and SO_2 values at the inlet and outlet of the device as,[22]

$$\dot{m}_{O_2} = \left[13.4 \cdot Hb\left(S_{O_2,out} - S_{O_2,in}\right) + \alpha \cdot 10^3\left(P_{O_2,out} - P_{O_2,in}\right)\right] \cdot Q_b \tag{5}$$

where Q_b is the volumetric blood flow rate and Hb is the total hemoglobin. The detailed modeling of the HFM bundle and

parameters used in the simulation can be found in Refs. [17,22].

4 | IN VITRO CHARACTERIZATION

Once the CFD analysis and iterative design of the PPL were completed, the geometry of the flow domain was divided into manufactured components. The 3D geometries of the components were designed for fabrication using CAD software. The PPL was first prototyped virtually and then with printed parts. The final components were injection molded from polycarbonate. The PPL was then assembled and tested in vitro experiments for hemolysis and gas transfer.

4.1 | Hemolysis

To investigate the hemolytic performance of the developed PPL, we used a small-volume (500 mL) circuit filled with fresh ovine blood, see the schematic diagram in Figure 4A. Fresh ovine blood was obtained by venipuncture from Lampire (Lampire Biological Laboratories, PA, USA) with a heparin concentration of 10 U/mL. An ECMO circuit consisting of the Quadrox-iD pediatric oxygenator and Rotaflow pump was also tested for comparison. The test was performed according to the protocol recommended by the American Society of Testing and Materials (ASTM F1841-19) to evaluate hemolysis in continuous blood flow pumps. The blood flow rate was set at 3.5 ± 0.2 L/min with an afterload pressure of 250 mm Hg, which yielded an impeller speed of 4000 rotations per minute (rpm) for the PPL and 3700 rpm for the Rotaflow pump. Hourly blood samples were collected during the 6-hour testing. Plasma was collected by centrifugation and measured for plasma-free hemoglobin (PFH). PFH concentration was determined by using a Hemoglobin Assay Kit (Catalog # MAK115, Millipore Sigma, St. Louis, MO, USA) with a SpectraMax M3 Spectrophotometer (Molecular Devices, San Jose, CA, USA). The normalized hemolysis index (NIH) was calculated according to ASTM F1841-19. More details on hemolysis experiment setting can be found in Ref. [23].

4.2 | Gas transfer

To characterize the oxygen transfer performance of the oxygenator, a mock flow loop was constructed; see the schematic diagram in Figure 4B. Filtered and heparinized ovine blood collected from a local abattoir was used. The hematocrit of the blood in the circuit was maintained at 36 ± 2%, and the temperature was maintained at 37 ± 1°C using a blood heat exchanger. In vitro gas transfer performance was evaluated according to ISO standard 7199.

Experiments were performed at different blood flow rates up to 4 L/min. Oxygenation of blood for the oxygenator was realized by flowing pure oxygen into the lumens of the fibers at a 1:1 ratio of oxygen to blood flow rate. Deoxygenation of blood was achieved by blowing a mixture of O_2, carbon dioxide (CO_2), and nitrogen (N_2) through the fiber of the oxygenator. Blood samples were taken at the ports before and after the oxygenator. The partial pressures of oxygen (PO_2), oxygen saturation (SO_2),

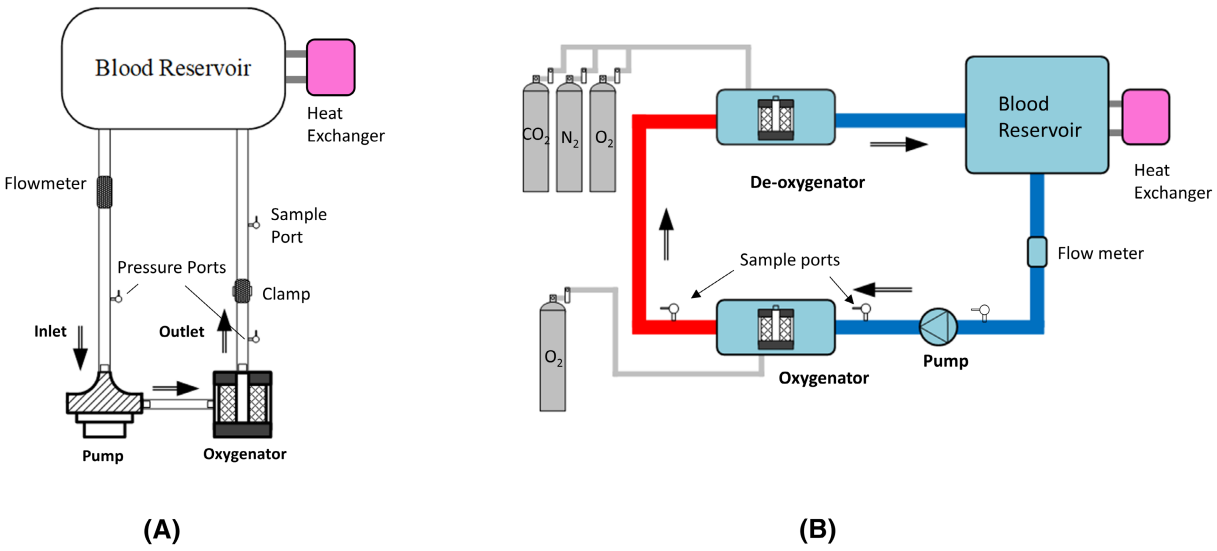

FIGURE 4 Schematic representation of the settings for the in vitro experiments. (A) Hemolysis and (B) gas transfer. [Color figure can be viewed at wileyonlinelibrary.com]

and other blood gas values were determined by analyzing the blood samples. More details on the gas transfer experiment setting can be found in Ref. [17].

5 | RESULTS

The pressure head versus flow rate (H-Q curves), that is, the pressure difference between inlet and outlet at a specified flow rate, is a crucial parameter for evaluating the hydrodynamic performance of a pump. Figure 5A presents the H-Q curves of the pediatric centrifugal pump at different rotational speeds. The pressure head of the pump predicted by CFD modeling agrees well with the experimental results (mean error of 2%), validating the accuracy of the meshing and the predictions established in the simulations. The results on the HQ curves indicate that the pump of PPL can provide adequate blood flow to pediatric patients across a range of physiological conditions. The pressure drop (loss) across the oxygenator at different flow rates was also investigated, as shown in Figure 5B. There is excellent agreement between the predicted CFD and experimental data, with the pressure loss increasing with the flow rate. Notably, the pressure drop was significantly lower in our new oxygenator than in the Quadrox-iD pediatric oxygenator at the same flow rate.[24] The afterload pressure of an ECMO can be calculated by subtracting the pressure drop across the oxygenator from the pressure head generated by the pump. Therefore, the PPL was able to achieve an afterload pressure of 250 mm Hg at a flow rate of 3.5 L/min with a rotational speed of 4000 rpm.

Figure 6 presents the pressure distribution and velocity contour with a vector field of the pump unit of the PPL on two cross sections at a flow rate of 3.5 L/min and an impeller speed of 4000 rpm. In Figure 6A, the axial incoming flow is guided by the cone and then changes its flow direction to radial, where it is accelerated by the impeller and enters the volute. Due to the diffusion of the volute, the blood flow slows down and pressurized by a portion of the kinetic energy (Figure 6B). Most of the blood is pumped to the outlet through the primary flow path. A small portion of the blood is driven by the pressure difference between the volute and the inlet, re-entering the impeller passage through the upper and lower gaps between the impeller and the pump housing, which are recognized as the secondary flow path. The distribution of SSS in the pump is illustrated in Figure 7. The majority of the fluid domain has SSS below 15 Pa, with high SSS (>50 Pa) occurring in areas where the blood flow undergoes a significant velocity change, such as near the inlet and outlet walls (spot 1, 200–300 Pa) and the tips of the impeller (spot 2, leading edge 250–350 Pa, trailing edge 150–200 Pa). High SSS also occurs on the walls of the secondary flow path (spot 3, top 150–200 Pa, bottom 100–150 Pa) as blood flows in the reverse direction into the narrow gaps.

Figure 8A shows the experimentally measured NIH of the PPL in comparison with the circuit consisting of the Rotaflow pump and the Quadrox-iD pediatric oxygenator. For the CFD comparison, HI was applied only to the pumps because the shear stress in the oxygenator is negligible. Figure 8B shows the CFD predicted one passage HI of the PPL pump (4000 rpm) compared with the Rotaflow pump (3700 rpm), at the same flow rate of 3.5 L/min. Detailed geometry and meshing schemes of the Rotaflow pump can be found in.[25] Both results suggest that the PPL has better hemolysis/biocompatibility performance than the Rotaflow pump with the Quadrox-iD pediatric oxygenator.

The fluid dynamics characteristics of the PPL oxygenator unit on a central plane at a flow rate of 3.5 L/min are shown in Figure 9. It exhibits a unique homogenous pressure distribution from the bottom to the top of the HFM bundle (Figure 8A). This unique pressure distribution is uniform from the outer surface to the inner surface of the HFM bundle. Due to this feature, the velocity field within the HFM bundle is nearly homogenously uniform in the radial direction from the outside to the inside, as illustrated in Figure 9B. The computationally predicted PO_2 and SO_2 distributions, along with the inlet and outlet values obtained in the in vitro experiment, are shown in Figure 9C,D, respectively. Both PO_2 and SO_2 increased as blood flow through the HFM bundle. Figure 10 displays the oxygen transfer rate of the PPL at various blood flow rates with a 1:1 ratio of sweep gas to blood flow rates. The computationally predicted O_2 transfer rates are in excellent agreement with the experimental results. The oxygen transfer rate increases linearly with increasing flow rate and reaches over 200 mL/min at a flow rate of 3.5 L/min.

6 | DISCUSSION

Despite the routine use of ECMO for cardiopulmonary failure, few devices are designed specifically for pediatric patients. No ECMO has been approved for long-term (>6 h) use by pediatric patients. ECMO systems for pediatric patients are adapted from those designed for adult use. Such use may be associated with increased blood cell damage, leading to hemolysis, thrombotic complications, and device failure. In previous efforts, our team successfully developed a wearable artificial pump-lung (APL) with a compact design,[26,27] which exhibited excellent biocompatibility, long-term reliability, and potential for bridging to lung transplantation in acute (24-hour) and 30-day in vivo experiments. However, the APL had high manufacturing costs due to its ultracompact design and maglev impeller.

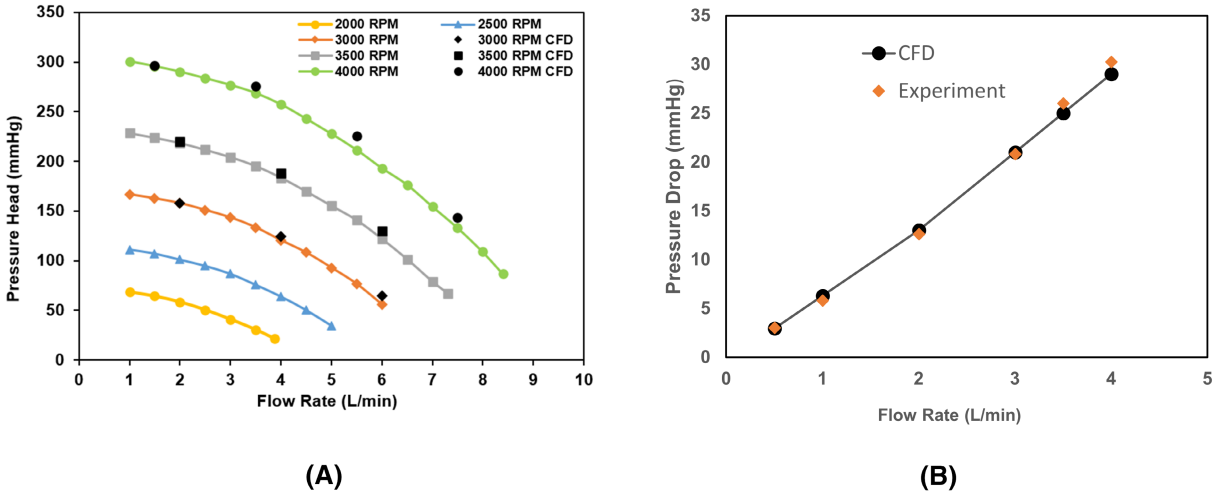

FIGURE 5 Pressure output in (A) the pump and (B) the oxygenator. [Color figure can be viewed at wileyonlinelibrary.com]

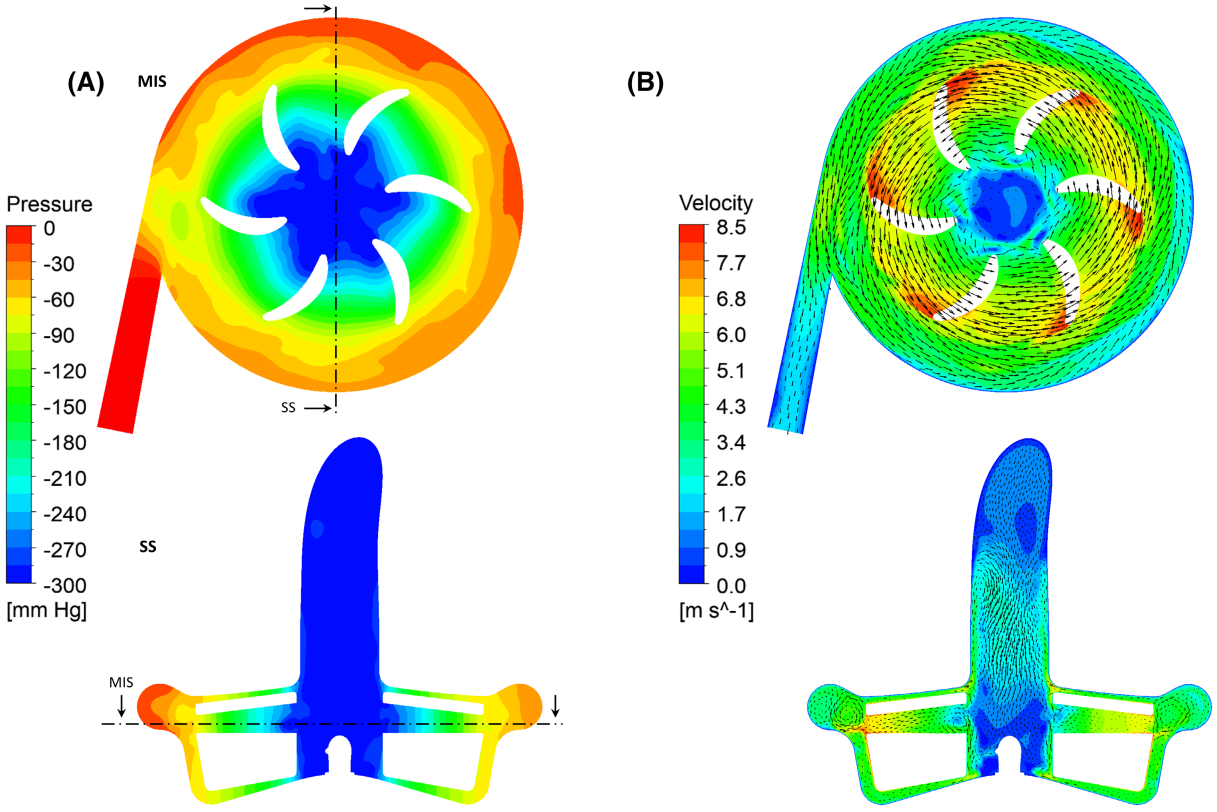

FIGURE 6 Fluid dynamic profiles of the PPL pump in two cross sections. (A) Pressure distribution and (B) velocity distribution with vector field. [Color figure can be viewed at wileyonlinelibrary.com]

To overcome this issue, we present the new PPL design, which consists of two separate modules, the pump and oxygenator, that can be easily integrated with each other. This modification significantly simplifies the manufacturing process. In addition, replacing the complex magnetic levitation bearing technology with a single cup-and-ball hybrid bearing further reduces the complexity and cost of the motor driver, making it a more practical solution for broader adoption.

The newly developed PPL was designed using CFD technology to optimize the fluid domain and minimize hemolysis while providing desirable respiratory support under targeted physiological conditions. Computational data were validated through in vitro mock studies using

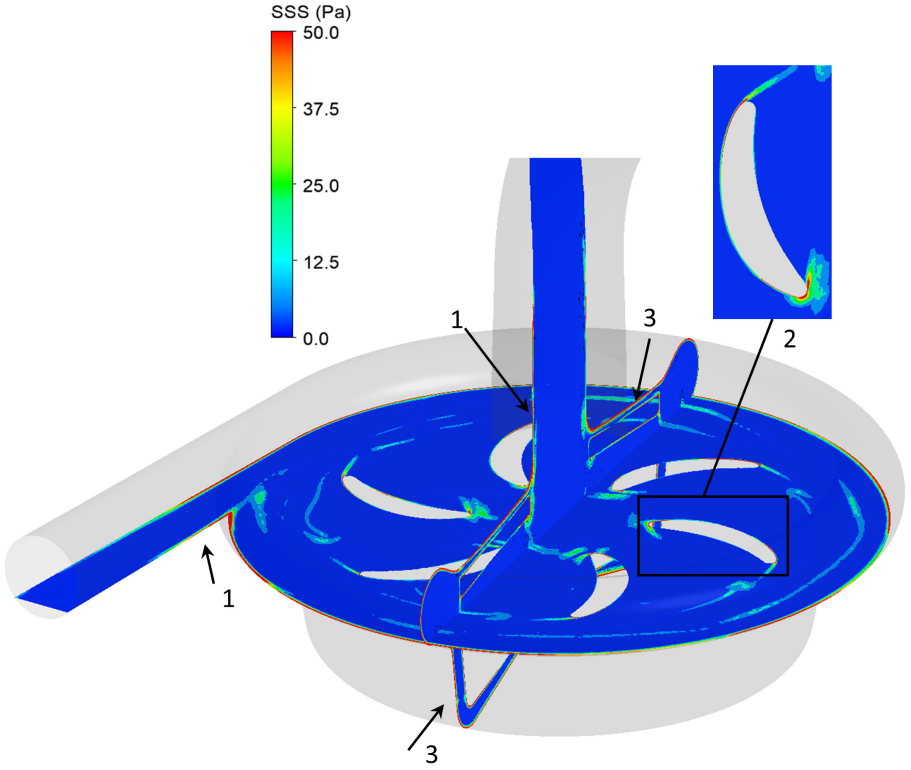

FIGURE 7 Scalar shear stress (SSS) distribution in the PPL pump. [Color figure can be viewed at wileyonlinelibrary.com]

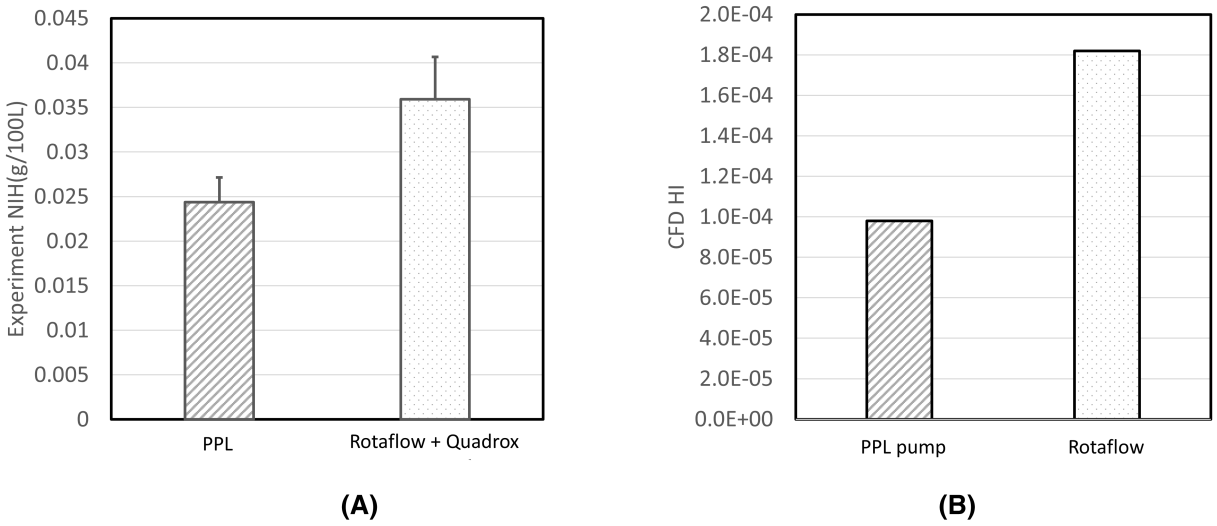

FIGURE 8 Comparison of (A) experimentally measured NIH of the PPL and Rotaflow connecting with a Quadrox-iD pediatric oxygenator at a flow rate of 3.5 L/min and an afterload pressure of 250 mm Hg, and (B) CFD-predicted HI in the PPL pump (at 4000 rpm) and Rotaflow (at 2800 rpm) under a flow rate of 3.5 L/min.

fresh ovine blood. Results demonstrate that PPL can provide respiratory/cardiopulmonary support with oxygen transfer over 200 mL/min at a flow rate of 3.5 L/min against an afterload pressure of 250 mm Hg. We did not specifically address CO_2 removal in this study. Since most CO_2 in the blood is dissolved or in the form of bicarbonate, it displays linear kinetics without saturation. CO_2 diffuses more readily than O_2 across extracorporeal membranes because its higher solubility. The rate of CO_2 removal in an oxygenator is generally proportional to the rate of O_2 transfer, and CO_2 can be effectively removed if the capacity of O_2 transfer in an oxygenator is sufficient. In addition, CFD-based and in vitro hemolysis analysis shows that the PPL exhibits superior biocompatibility compared to a combination of the Quadrox-iD pediatric oxygenator and Rotaflow pump under the same physiological

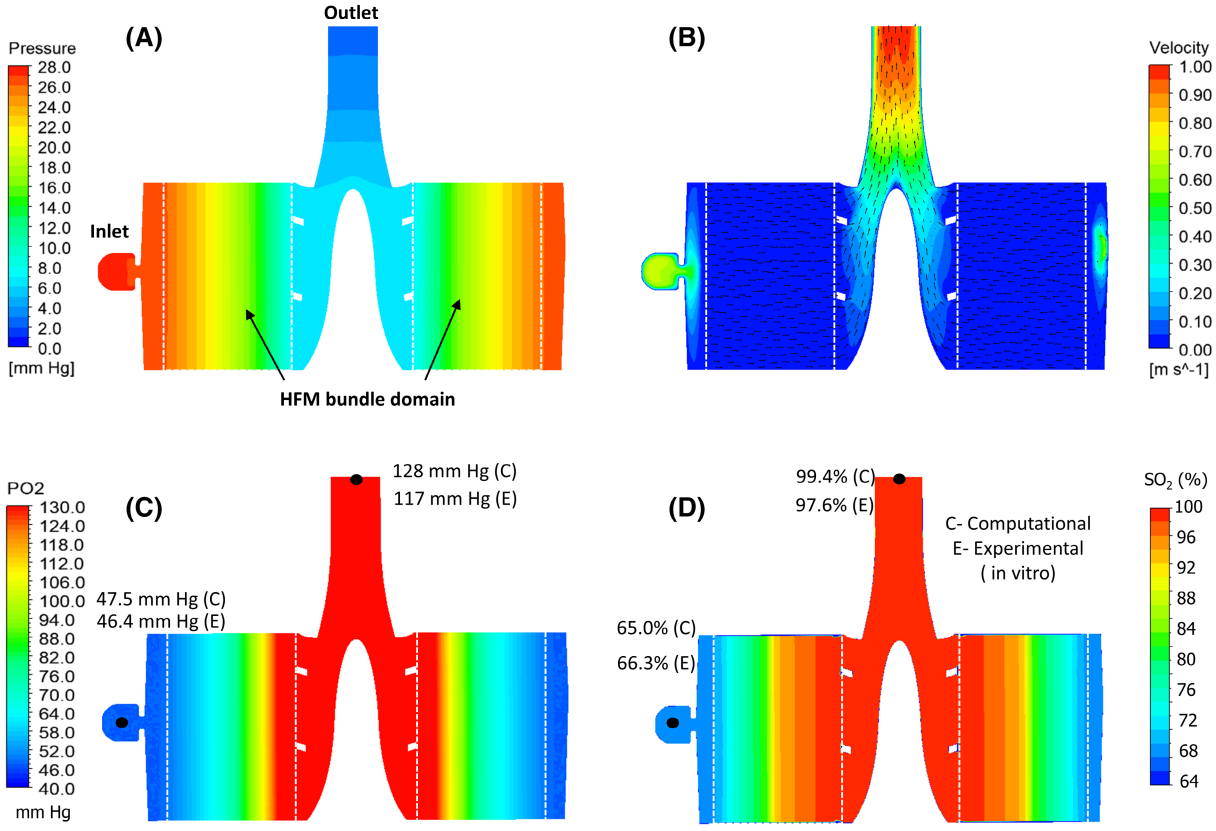

FIGURE 9 Cross-sectional view of blood flow and oxygen transfer characteristics in the oxygenator. (A) Pressure distribution; (B) velocity distribution with vector; (C) PO_2, and (D) SO_2 distribution with experimentally measured values in the outlet and inlet. [Color figure can be viewed at wileyonlinelibrary.com]

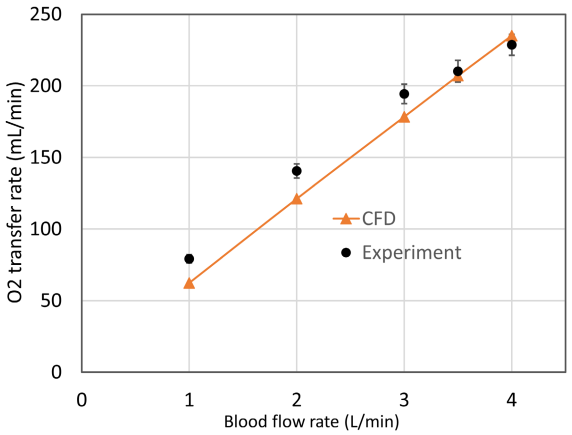

FIGURE 10 Oxygen transfer in PPL at different blood flow rates. [Color figure can be viewed at wileyonlinelibrary.com]

operating conditions (afterload pressure of 250 mm Hg at a flow rate of 3.5 L/min). The unique flow path of the PPL oxygenator unit reduces resistance throughout the circulation and requires less force to move blood through the system, resulting in reduced damage to blood cells. These findings provide evidence of the newly developed PPL's effectiveness and suitability for clinical use. Ongoing 30-day in vivo animal experiments will further evaluate its safety and efficacy.

The shear stress-induced blood damage (e.g., hemolysis) is primarily caused by the pump. Specifically, the impeller tips experience higher shear stress levels due to the rotational motion of the blades against the flow in the normal direction, which creates higher velocity gradients near the blade tips. When operating at the off-design point, particularly at high rotating speeds, an increase in hemolysis can be expected due to elevated shear stress levels and flow interactions at the interface between the impeller and pump housing. Beside the damage to the red blood cells, optimizing the device for long-term use will require further investigation into shear-induced damage to other critical blood components such as platelets, leukocytes, and von Willebrand factor.

7 | CONCLUSION

In this study, we utilized CFD-based multidisciplinary modeling to analyze and design the PPL for oxygen transfer performance and biocompatibility. The ovine blood-based in vitro mock experiments were conducted to characterize

the PPL. The results of the computationally predicted and in vitro tests demonstrated that this novel device could provide respiratory/cardiopulmonary support to pediatric patients with respiratory failure with an acceptable level of hemolysis. Our findings suggest that CFD-based modeling can be an effective tool for predicting the flow field, pressure distribution, and oxygen transfer in the design of new ECMO systems. Furthermore, the use of fresh ovine blood in these experiments allowed for the validation of gas transfer efficiency and biocompatibility, providing reliable data prior to in vivo experiments and clinical trials. The PPL has the potential to provide superior respiratory support with minimal risk of hemolysis.

AUTHOR CONTRIBUTIONS

Dong Han: Conceptualization, Data collection and analysis, Manuscript writing. **Jiafeng Zhang**: Conceptualization, Data collection, Manuscript reviewing, and editing. **Ge He**: Conceptualization and Manuscript reviewing. **Bartley P. Griffith**: Securing funding and Manuscript reviewing. **Zhongjun J. Wu**: Conceptualization, Securing funding, Manuscript reviewing, and editing.

ACKNOWLEDGMENTS

This work was partially funded by National Institutes of Health (Grant Numbers: R01HL118372, R01HL124170, R01HL141817, and R01HL162940).

CONFLICT OF INTEREST STATEMENT

Zhongjun J. Wu and Bartley P. Griffith disclose financial interest in Abiomed-Breethe, Inc. and intellectual property in ECMO systems, blood pumps, and relevant enabling technologies. Jiafeng Zhang discloses financial interest in intellectual property for ECMO systems and blood pumps. Zhongjun J. Wu serves a consultant to Daiichi Sankyo, Inc. and CH Biomedical USA, inc. All other authors declare that they have no conflict of interest in the subject matter and materials reported in this study.

ORCID

Zhongjun J. Wu https://orcid.org/0000-0003-0807-7195

REFERENCES

1. Kenneth D, Kochanek SM, Jiaquan X, Arias E. Mortality in the United States, 2016. NCHS Data Brief. 2017 Dec;293:1–8.
2. Bellani G, Laffey JG, Pham T, Fan E, Brochard L, Esteban A, et al. Epidemiology, patterns of care, and mortality for patients with acute respiratory distress syndrome in intensive care units in 50 countries. JAMA. 2016;315(8):788–800.
3. Yehya N, Thomas NJ. Relevant outcomes in pediatric acute respiratory distress syndrome studies. Front Pediatr. 2016;4:51.
4. https://www.who.int/news-room/fact-sheets/detail/pneumonia.
5. Valencia E, Nasr VG. Updates in pediatric extracorporeal membrane oxygenation. J Cardiothorac Vasc Anesth. 2020;34(5):1309–23.
6. Jenks CL, Raman L, Dalton HJ. Pediatric extracorporeal membrane oxygenation. Crit Care Clin. 2017;33(4):825–41.
7. Erdil T, Lemme F, Konetzka A, Cavigelli-Brunner A, Niesse O, Dave H, et al. Extracorporeal membrane oxygenation support in pediatrics. Ann Cardiothorac Surg. 2019;8(1):109–15.
8. Shih E, Michael DiMaio J, Squiers JJ, Banwait JK, Kussman HM, Meyers DP, et al. Bloodstream and respiratory coinfections in patients with COVID-19 on ECMO. J Card Surg. 2022;37:3609–18.
9. Dahlberg P, Prekker M, Hertz M, Herrington C, Park S. Medium term results of ECMO for severe acute lung injury following lung transplantation. J Heart Lung Transplant. 2003;22(1):S159–60.
10. Papanastasiou CA, Kyriakoulis KG, Theochari CA, Kokkinidis DG, Karamitsos TD, Palaiodimos L. Comprehensive review of hemolysis in ventricular assist devices. World J Cardiol. 2020;12(7):334–41.
11. Tarzia V, Buratto E, Bortolussi G, Gallo M, Bejko J, Bianco R, et al. Hemorrhage and thrombosis with different LVAD technologies: a matter of flow? Ann Cardiothorac Surg. 2014;3(6):582–4.
12. Blombäck M, Kronlund P, Åberg B, Fatah K, Hansson L-O, Egberg N, et al. Pathologic fibrin formation and cold-induced clotting of membrane oxygenators during cardiopulmonary bypass. J Cardiothorac Vasc Anesth. 1995;9(1):34–43.
13. Fukuda M, Tokumine A, Noda K, Sakai K. Newly developed pediatric membrane oxygenator that suppresses excessive pressure drop in cardiopulmonary bypass and extracorporeal membrane oxygenation (ECMO). Membranes. 2020;10(11):362.
14. Faghih MM, Keith SM. Extending the power-law hemolysis model to complex flows. J Biomech Eng. 2016;138(12):124504.
15. Taskin ME, Fraser KH, Zhang T, Wu C, Griffith BP, Wu ZJ. Evaluation of Eulerian and Lagrangian models for hemolysis estimation. ASAIO J. 2012;58(4):363–72.
16. Han D, Zhang J, Griffith BP, Wu ZJ. Models of shear-induced platelet activation and numerical implementation with computational fluid dynamics approaches. J Biomech Eng. 2022;144(4):040801.
17. Zhang J, Nolan TD, Zhang T, Griffith BP, Wu ZJ. Characterization of membrane blood oxygenation devices using computational fluid dynamics. J Membr Sci. 2007;288(1–2):268–79.
18. Han D, Shah A, Awad MA, Wu ZJ, Griffith BP. Development of an ambulatory extracorporeal membrane oxygenation system: from concept to clinical use. Appl Eng Sci. 2022;10:100093.
19. Zhang J, Zhang P, Fraser KH, Griffith BP, Wu ZJ. Comparison and experimental validation of fluid dynamic numerical models for a clinical ventricular assist device. Artif Organs. 2013;37(4):380–9.
20. Ding J, Niu S, Chen Z, Zhang T, Griffith BP, Wu ZJ. Shear-induced hemolysis: species differences. Artif Organs. 2015;39(9):795–802.
21. Chen Z, Jena SK, Giridharan GA, Koenig SC, Slaughter MS, Griffith BP, et al. Flow features and device-induced blood trauma in CF-VADs under a pulsatile blood flow condition: a CFD comparative study. Int J Numer Method Biomed Eng. 2018;34(2):e2924.

22. Ertan Taskin M, Zhang T, Fraser KH, Griffith BP, Wu ZJ. Design optimization of a wearable artificial pump-lung device with computational modeling. J Med Devices. 2012;6(3):031009.
23. Berk ZB, Zhang J, Chen Z, Tran D, Griffith BP, Wu ZJ. Evaluation of in vitro hemolysis and platelet activation of a newly developed maglev LVAD and two clinically used LVADs with human blood. Artif Organs. 2019;43(9):870–9.
24. MAQUET. Getinge Group, Quadrox-iD pediatric product presentation. Available from: https://www.cardiomedic.com.ar/Brochure/ecmo-pls-pediatrico.pdf
25. He G, Zhang J, Shah A, Berk ZB, Han L, Dong H, et al. Flow characteristics and hemolytic performance of the new Breethe centrifugal blood pump in comparison with the CentriMag and Rotaflow pumps. Int J Artif Organs. 2021;44(11):829–37.
26. Wu ZJ, Taskin ME, Zhang T, Fraser KH, Griffith BP. Computational model-based design of a wearable artificial pump-lung for cardiopulmonary/respiratory support. Artif Organs. 2012;36(4):387–99.
27. Wu ZJ, Zhang T, Bianchi G, Wei X, Son H-S, Zhou K, et al. Thirty-day in-vivo performance of a wearable artificial pump-lung for ambulatory respiratory support. Ann Thorac Surg. 2012;93(1):274–81.

How to cite this article: Han D, Zhang J, He Ge, Griffith BP, Wu ZJ. Computational fluid dynamics-based design and in vitro characterization of a novel pediatric pump-lung. Artif. Organs. 2024;48:130–140. https://doi.org/10.1111/aor.14665